Figure S1

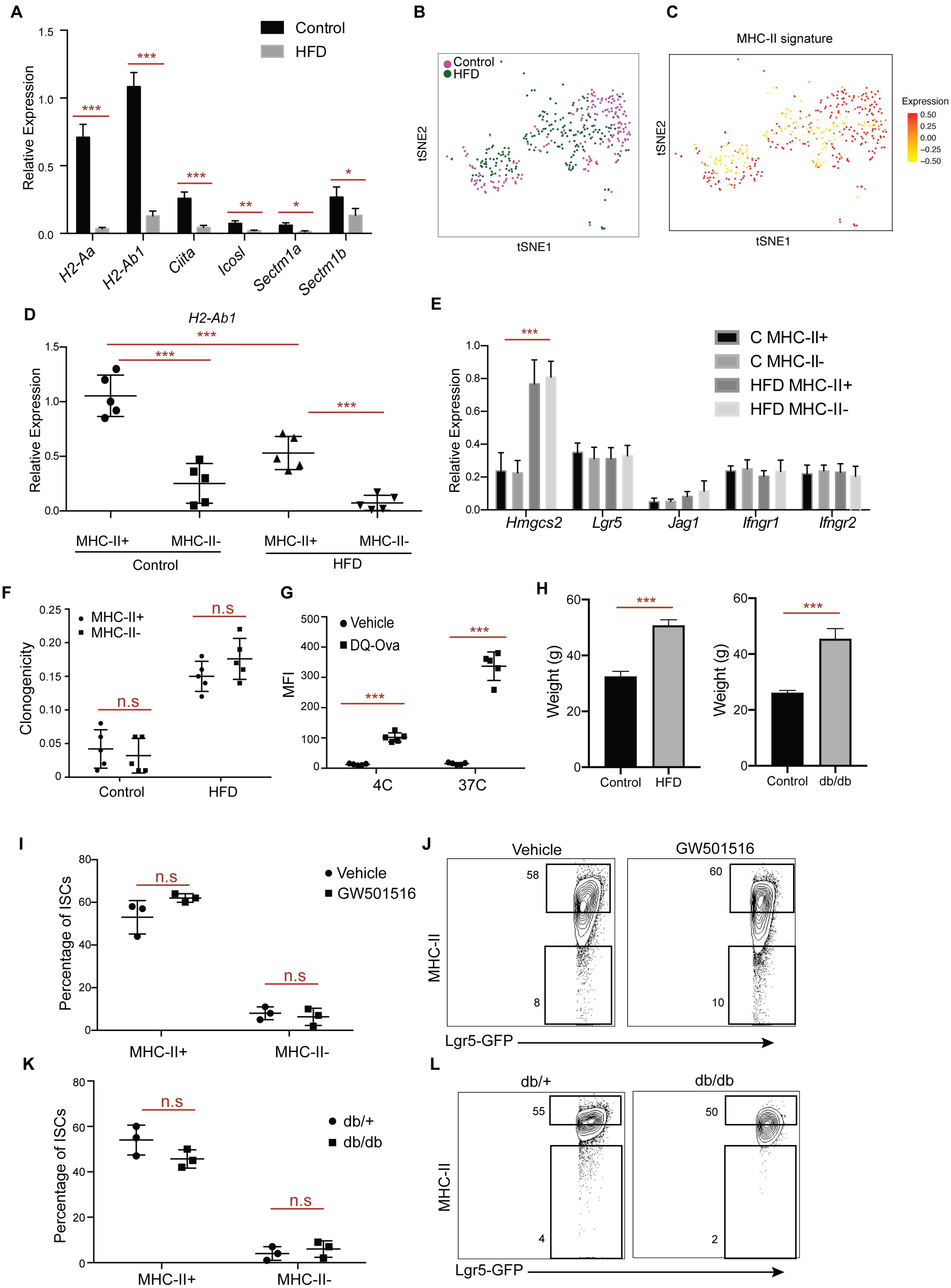

A
Control
HFD
Relative Expression
H2-Aa
H2-Ab1
Ciita
Icosl
Sectm1a
Sectm1b
B
Control
HFD
tSNE1
tSNE2
C
MHC-II signature
Expression
tSNE1
tSNE2
D
H2-Ab1
Relative Expression
MHC-II+
MHC-II-
Control
HFD
E
C MHC-II+
C MHC-II-
HFD MHC-II+
HFD MHC-II-
Relative Expression
Hmgcs2
Lgr5
Jag1
Ifngr1
Ifngr2
F
MHC-II+
MHC-II-
Clonogenicity
n.s
Control
HFD
G
Vehicle
DQ-Ova
MFI
4C
37C
H
Weight (g)
Control
HFD
db/db
I
Percentage of ISCs
Vehicle
GW501516
MHC-II+
MHC-II-
J
Vehicle
GW501516
MHC-II
Lgr5-GFP
K
Percentage of ISCs
db/+
db/db
MHC-II+
MHC-II-
L
db/+
db/db
MHC-II
Lgr5-GFP

Supplementary Figure 1. Characterization of MHC-II expression in ISCs, related to Figure 1.

A. Relative expression of immunomodulatory genes in control and HFD Lgr5+ ISCs (*n*=5).

B. *t*-Distributed stochastic neighbour embedding (tSNE) analysis of single Lgr5+ ISCs isolated from control (n=171 cells, 2 independent experiments) or HFD mice (n=144 cells, 2 independent experiments).

C. tSNE analysis of single cells using MHC-II pathway signature genes (Supplementary Table 1)

D. Relative expression of MHC-II (*H2-Ab1*) in control and HFD MHC-II+ and MHC-II- Lgr5+ ISCs (*n*=5).

E. Relative expression of signature PPAR-δ target (*Hmgcs2*), stem cell marker (*Lgr5*), PPAR-δ -dependent B-catenin target (*Jag1*) and IFNGR genes in control and HFD MHC-II+ and MHC-II- Lgr5+ ISCs (*n*=5).

F. Organoid-initiating capacity of MHC-II+ and MHC-II- Lgr5+ ISCs from HFD mice (*n*=5).

G. Mean fluorescence intensity (MFI) of ISCs pulsed with either vehicle or DQ-Ovalbumin for 8 hours at 4C and 37C (*n*=5, 3 technical replicates per experiment).

H. Weight of mice used for diet-induced obesity (left: Control and HFD, *n*=15) and leptin receptor deficiency models of obesity (right, Control and db/db, *n*=7) in the study.

I, J. Frequency of MHC-II+ and MHC-II- Lgr5+ ISCs in vehicle- and PPAR-δ agonist GW501516-treated mice by flow cytometry (**I**, *n*=3). Representative flow cytometry plots of MHC-II in vehicle- and PPAR-δ agonist GW501516-treated Lgr5+ ISCs **(J)**.

K, L. Frequency of MHC-II+ and MHC-II- Lgr5+ ISCs in lean db/+ and obese db/db mice (**K**, *n*=3). Representative flow cytometry plots of MHC-II+ and MHC-II- Lgr5+ ISCs (**l**, *n*=3).

Unless otherwise indicated, data are mean ± s.d. from *n* independent experiments; n.s.: not significant, *$P < 0.05$, **$P < 0.01$, ***$P < 0.001$ (Student's *t*-tests).

Related to Figure 1.

Figure S2

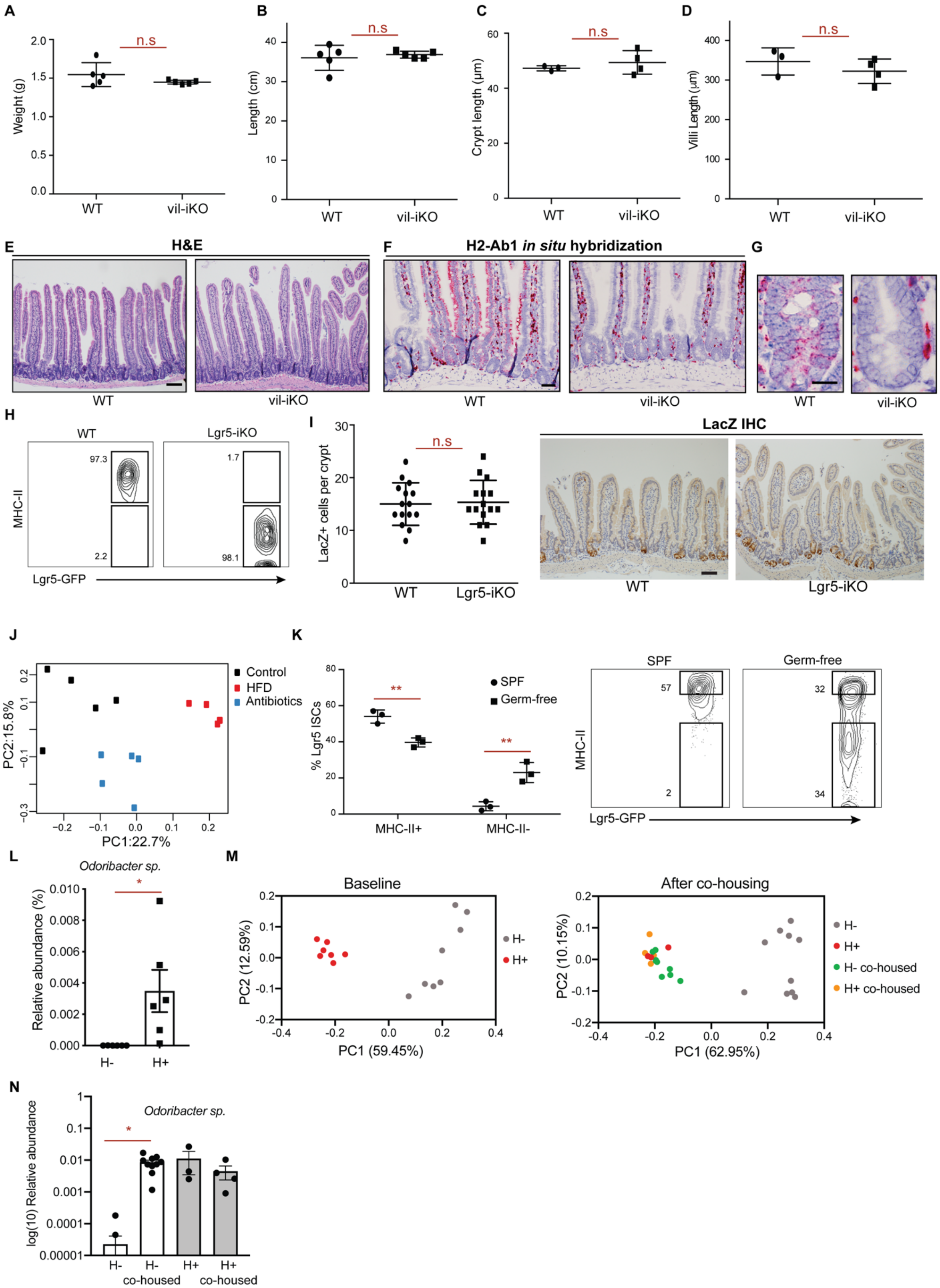

A
n.s
Weight (g)
WT
vil-iKO
B
n.s
Length (cm)
WT
vil-iKO
C
n.s
Crypt length (µm)
WT
vil-iKO
D
n.s
Villi Length (µm)
WT
vil-iKO
E
H&E
WT
vil-iKO
F
H2-Ab1 *in situ* hybridization
WT
vil-iKO
G
WT
vil-iKO
H
WT
Lgr5-iKO
MHC-II
Lgr5-GFP
97.3
2.2
1.7
98.1
I
n.s
LacZ+ cells per crypt
WT
Lgr5-iKO
LacZ IHC
WT
Lgr5-iKO
J
Control
HFD
Antibiotics
PC2:15.8%
PC1:22.7%
K
SPF
Germ-free
% Lgr5 ISCs
MHC-II+
MHC-II-
SPF
Germ-free
57
2
32
34
MHC-II
Lgr5-GFP
L
Odoribacter sp.
Relative abundance (%)
H-
H+
M
Baseline
PC2 (12.59%)
PC1 (59.45%)
H-
H+
After co-housing
PC2 (10.15%)
PC1 (62.95%)
H-
H+
H- co-housed
H+ co-housed
N
Odoribacter sp.
log(10) Relative abundance
H-
H-
co-housed
H+
H+
co-housed

Supplementary Figure 2. Intestine-specific deletion of MHC-II does not alter intestinal physiology and microbiome regulates epithelial MHC-II expression, related to Figures 2, 3 and 4.

A-**E**, Intestinal weight (**A**, *n*=5), length (**B**, *n*=5), crypt (**C**, *n*=5), and villi length (**D**, *n*=5) of MHC-II wild type (WT) and MHC-II$^{L/L}$; Villin-CreERT2 (vil-iKO) mice one month after tamoxifen injection (n= mice, mean ± s.d.). Representative H&Es of WT and vil-iKO small intestine (**E**).

F, **G**, *In situ* hybridization for *H2-Ab1* in the intestine (**F**) and representative images of intestinal crypts (**G**) in WT and vil-iKO mice (*n*=3).

H. Frequencies of MHC-II+ and MHC-II- Lgr5+ ISCs in WT and MHC$^{L/L}$; Lgr5-CreERT2 (Lgr5-iKO) by flow cytometry (*n*=5 mice).

I. Lineage tracing of LacZ+ cells in the intestinal crypt after deletion of MHC-II in ISCs (left). Representative images of LacZ immunostain in WT and Lgr5-iKO small intestine (right) (n=5 mice).

J. Principal coordinate analysis (PCoA) of microbial composition in feces of mice fed control diet, HFD, and mice treated with antibiotics (*n*=5 mice).

K. Frequencies of MHC-II+ and MHC-II- Lgr5+ ISCs in specific-pathogen free (SPF) and germ-free mice by flow cytometry (*n*=3, mean ± s.d.). Representative flow cytometry plots of MHC-II in SPF and germ-free ISCs.

L. Relative abundance of *Odoribacter sp.* in mice housed in H- room or H+ room (*n*=6, mean ± s.e.m).

M. PCoA of microbial composition in feces at baseline level before co-housing experiment (left) and 10 days after co-housing H- mice with H+ mice in the H+ room.

N. Relative abundance of *Odoribacter sp.* in feces of mice housed either in H- room (*n*=10), H+ room (*n*=3), or after co-housing H- mice (*n*=10) with H+ mice (*n*=4) in H+ room (mean ± s.e.m).

n.s.: not significant, **P* < 0.05, ***P* < 0.01(Student's *t*-tests). Scale bars, 100 μm (**E**), 50 μm (**F**, **I**) and 20 μm (**G**).

Figure S3

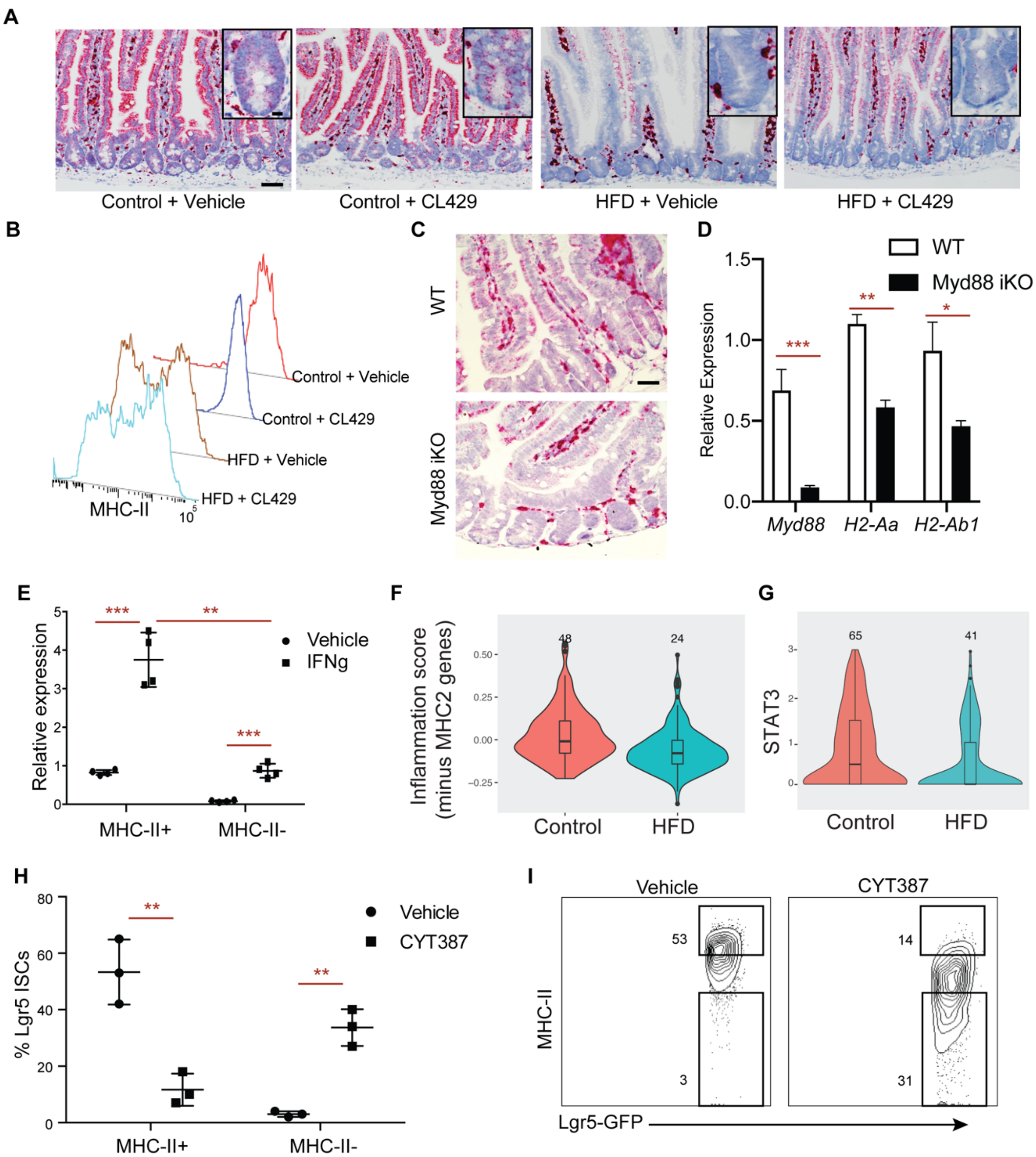

Supplementary Figure 3. Regulation of MHC-II expression in ISCs by PRR and IFNγ signaling, related to Figure 5.

A, B. *In situ* hybridization for H2-Ab1 in control and HFD mice treated with vehicle- and CL429-treated mice in proximal small intestine (**A**, *n*=3). Representative histogram plots of MHC-II in Lgr5+ ISCs in control and HFD mice treated with vehicle and CL429 (**B**, *n*=3).

C. *In situ* hybridization for H2-Ab1 in WT and Myd88 KO mice (*n*=4).

D. Relative expression of *Myd88* and MHC-II genes (*H2-Aa* and *H2-Ab1*) in the intestine from WT and Myd88 KO mice (*n*=5, mean ± s.d.).

E. Relative expression of MHC-II (*H2-Ab1*) in MHC-II+ and MHC-II- Lgr5+ ISCs isolated from HFD mice with or without IFNg stimulation (*n*=4, mean ± s.d.).

F. Violin plots demonstrating the levels of IFNg-induced genes excluding MHC-II pathway genes in control and HFD Lgr5+ ISCs by scRNA-seq.

G. Violin plots demonstrating the levels of STAT3 in control and HFD Lgr5+ ISCs by scRNA-seq.

H, I. Frequencies of MHC-II+ and MHC-II- Lgr5+ ISCs in vehicle- and Jak/Stat inhibitor CYT387-treated mice (*n*=3). Representative flow cytometry plots of MHC-II in vehicle- and CYT387-treated Lgr5+ ISCs (**I**).

Unless otherwise indicated, data are from *n* independent experiments; *$P < 0.05$, **$P < 0.01$, ***$P < 0.001$ (Student's *t*-tests). Scale bars, 50 μm (**A, C**) and 20 μm (insets, **A**).

Figure S4

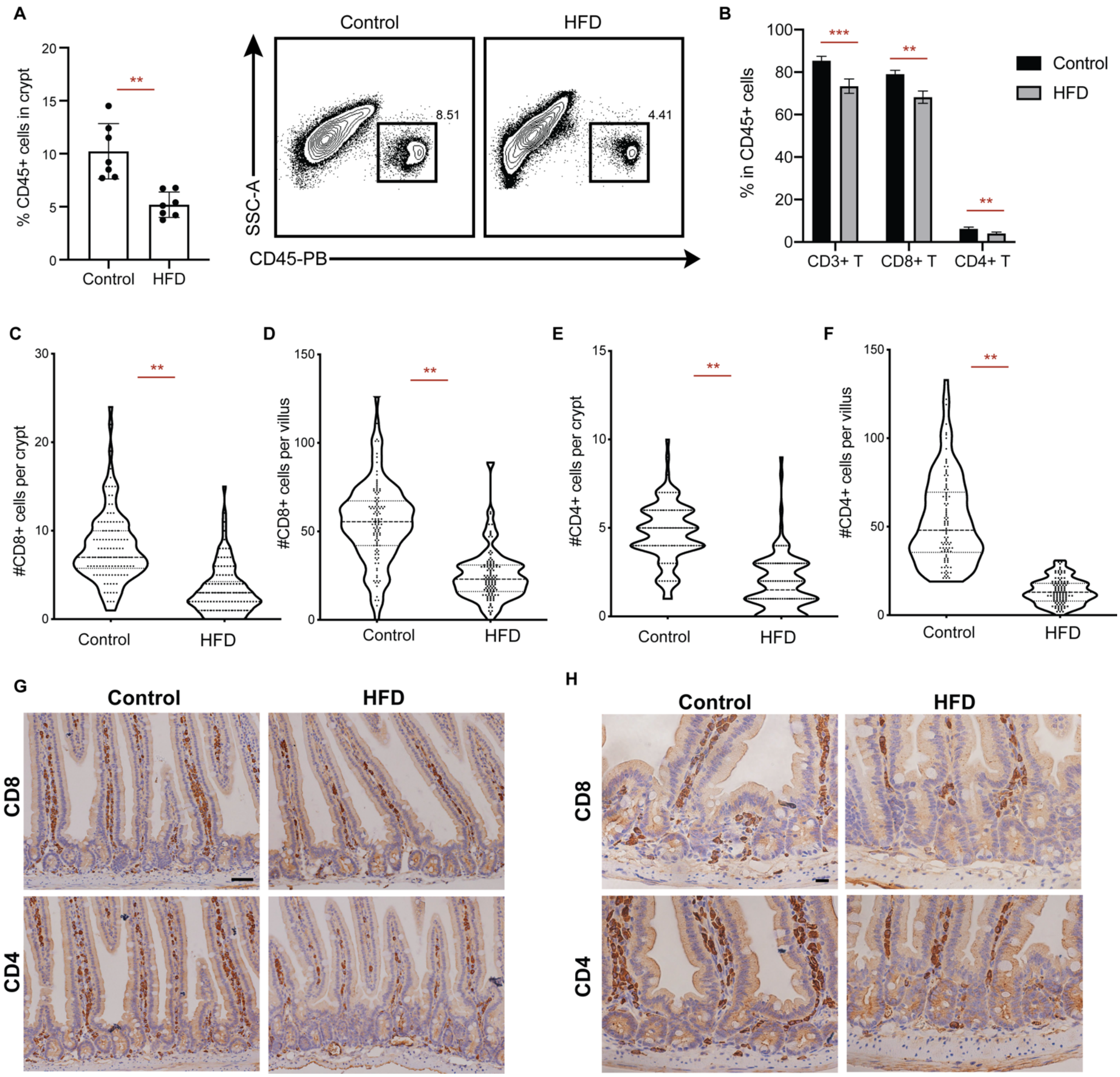

Supplementary Figure 4. The effect of HFD on intestinal immune cells, related to Figure 5.

A. Frequency of CD45+ cells in intestinal crypts isolated from control or HFD mice (n=7).

B. Frequency of CD3+ T cells, CD8+ T cells and CD4+ T cells among CD45+ cells in intestinal crypts isolated from control or HFD mice (*n*=5).

C-H. Numbers of CD8+ cells (**C**, crypt; **D**, villus) and CD4+ cells (**E**, crypt; **F**, villus) in the intestines of control or HFD mice. Representative images of CD4 and CD8 immunostaining in control or HFD intestines (**G**, **H**) (n=5). $^{**}P < 0.01$, $^{***}P < 0.001$ (Student's *t*-tests). Scale bars, 50 μm (**G**) and 20 μm (**H**).

Figure S5

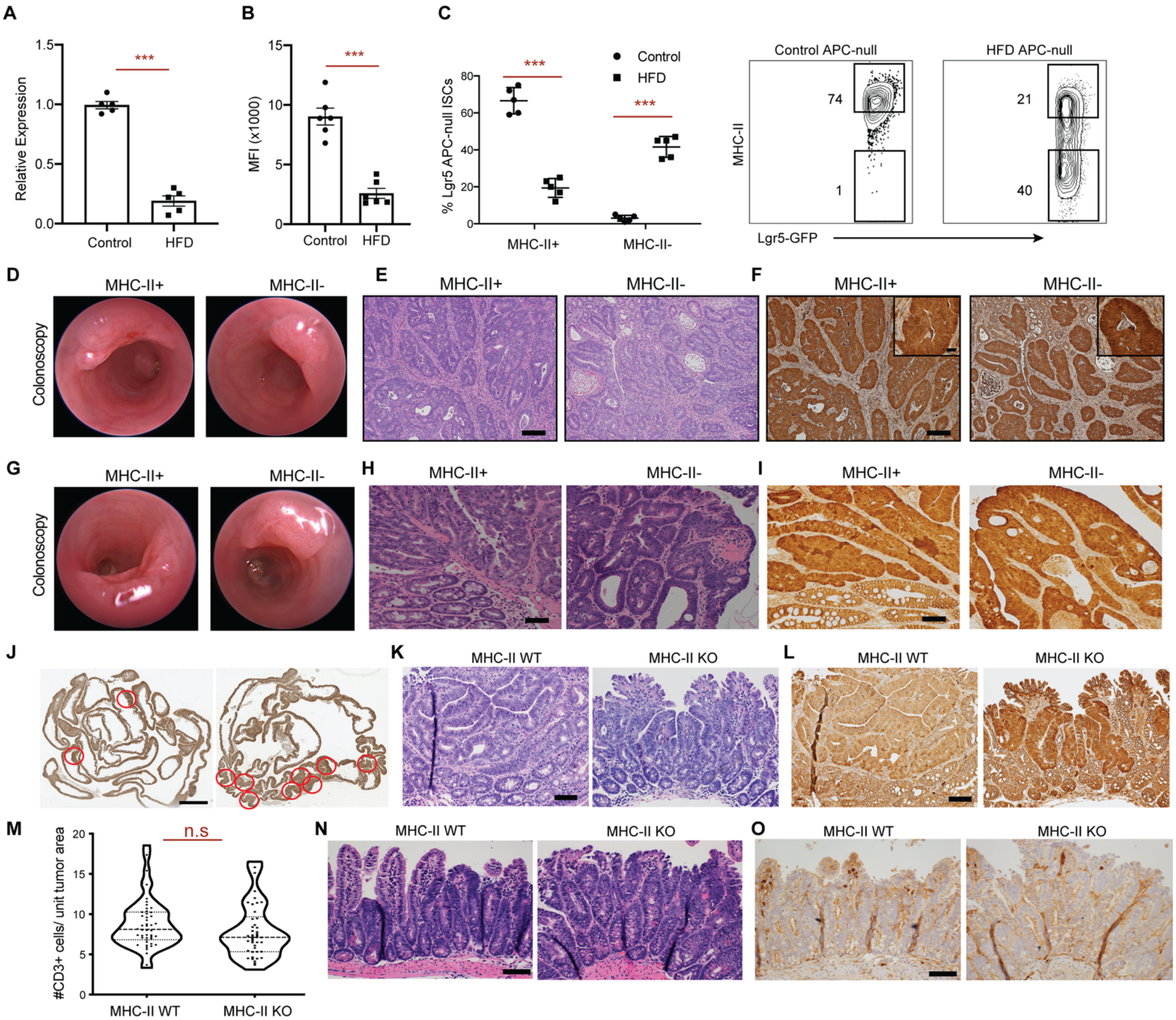

Supplementary Figure 5. The effect of Lgr5+ ISC MHC-II expression on tumor formation, related to Figure 6.

A. Relative expression of MHC-II (*H2-Ab1*) in Lgr5+ *Apc*-null pre-malignant ISCs isolated from control or HFD mice 3 days post tamoxifen injection (*n*=5).

B. Mean fluorescence intensity (MFI) of MHC-II in Lgr5+ *Apc*-null pre-malignant ISCs isolated from control or HFD mice 3 days post tamoxifen injection (*n*=6).

C. Frequency of MHC-II+ and MHC-II- Lgr5+ *Apc*-null ISCs in control and HFD mice by flow cytometry (*n*=5). Representative flow cytometry plots of MHC-II in HFD *Apc*-null ISCs.

D-F. Characterization of orthotopically transplanted MHC-II+ and MHC-II- *Apc*-null Lgr5+ ISCs-derived tumors three months after transplantation into immunocompetent syngeneic hosts. Optical colonoscopy images (**D**), Hematoxylin and eosin (**E**) and beta-catenin immunostain (**F**) of tumors.

G-I. Characterization of orthotopically transplanted MHC-II+ and MHC-II- *Apc*-null Lgr5+ ISCs-derived tumors three months after transplantation into immunodeficient Rag2-KO hosts. Optical colonoscopy images (**G**), H&E (**H**) and beta-catenin immunostain (**I**) of tumors.

J-L. Tumors in Lgr5-CreERT2 MHC-II$^{L/+}$, APC$^{L/+}$ (*n*=9, MHC-II WT APC-het) and Lgr5-CreERT2 MHC-II$^{L/L}$, APC$^{L/+}$ (*n*=9, MHC-II KO APC-het). Representative images of tumors that arise in MHC-II WT (**J,** left) and MHC-II KO (**J**, right) mice. Representative H&E (**K**) and beta-catenin immunostain (**L**) images from tumors in MHC-II WT and MHC-II KO mice.

M-O. Numbers of CD3+ T cells per tumor area (**M**). Representative H&E (**N**) and CD3 immunostain (**O**) images from tumors (n=5). n.s.: not significant, ***$P < 0.001$ (Student's *t*-tests). Scale bars, 100 μm (**E, F, H, I, K, L, N, O**) and 20 μm (insets, **F**).

Figure S6

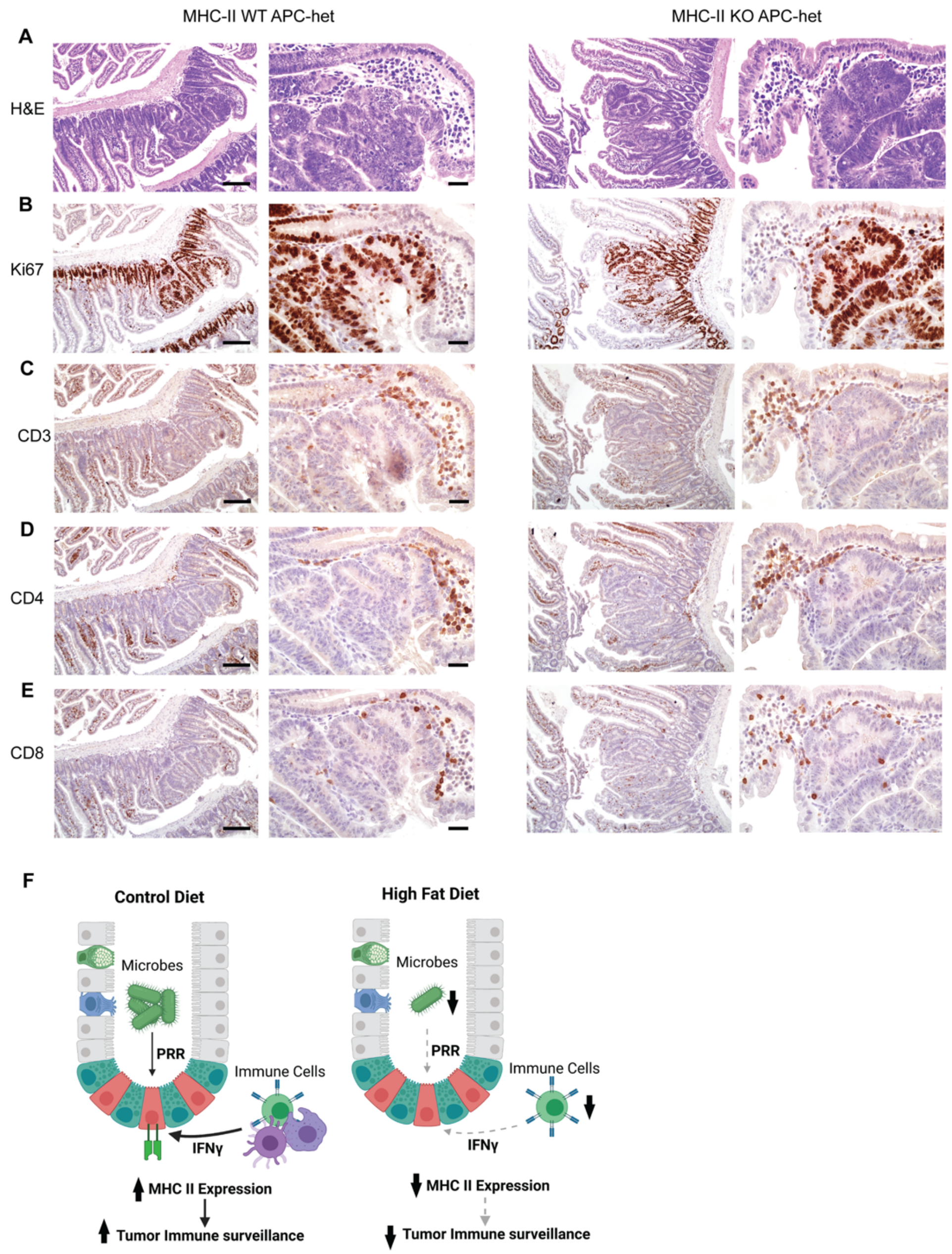

Supplementary Figure 6. Immune cell profile of tumors that arise upon intestine specific deletion of MHC-II and *Apc*, related to Figure 6.

A-E. Representative H&E (**A**), Ki67 (**B**), CD3 (**C**), CD4 (**D**) and CD8 (**E**) immunostain images of tumors in Lgr5-CreERT2 MHC-II$^{L/+}$, APC$^{L/+}$ (MHC-II WT APC-het) and Lgr5-CreERT2 MHC-II$^{L/L}$, APC$^{L/+}$ (MHC-II KO APC-het) mice. Scale bars, 500 µm (left, **A – E**), 100 µm (right, **A – E**).

F. Model of dietary regulation of intestinal tumor initiation through perturbing microbe – stem cell – immune cell crosstalk. Intestinal microbiome, Pattern Recognition Receptor (PRR) and IFNγ signaling regulate epithelial MHC-II expression and tumor immune surveillance in control diet fed mice (left). A HFD leads to microbial dysbiosis and dampened MHC-II expression that results in impaired tumor immune surveillance and increased tumor initiation.

Supplementary Table S1: The list of genes defining the stem cell MHC-II signature. Related to Figure 1.

Stem Cell MHC-II Signature
H2-Ab1
H2-DMb1
H2-DMa
H2-Aa
CD74
Ciita
H2-Eb1
Ceacam10
Cd177
Cd320

Supplementary Table S2: The list of microbes that colonize mice in H+ room. Related to Figure 4.

	H- Room	H+ Room
Helicobacter spp.	-	+
Helicobacter mastomyrinus	-	+
Helicobacter typhlonius	-	+

Supplementary Table S3: The list of qRT-PCR primers. Related to the STAR Methods.

TLR1(F): TGAGGGTCCTGATAATGTCCTAC
TLR1(R): AGAGGTCCAAATGCTTGAGGC
TLR2(F): GCAAACGCTGTTCTGCTCAG
TLR2(R): AGGCGTCTCCCTCTATTGTATT
TLR3(F): GTGAGATACAACGTAGCTGACTG
TLR3(R): TCCTGCATCCAAGATAGCAAGT
TLR4(F): ATGGCATGGCTTACACCACC
TLR4(R): GAGGCCAATTTTGTCTCCACA
TLR5(F): GCAGGATCATGGCATGTCAAC
TLR5(R): ATCTGGGTGAGGTTACAGCCT
TLR6(F): TGAGCCAAGACAGAAAACCCA
TLR6(R): GGGACATGAGTAAGGTTCCTGTT
TLR7(F): ATGTGGACACGGAAGAGACAA
TLR7(R): GGTAAGGGTAAGATTGGTGGTG
TLR8(F): GAAAACATGCCCCCTCAGTCA
TLR8(R): CGTCACAAGGATAGCTTCTGGAA
TLR9(F): ATGGTTCTCCGTCGAAGGACT
TLR9(R): GAGGCTTCAGCTCACAGGG
Nod1(F): GAAGGCACCCCATTGGGTT
Nod1(R): AATCTCTGCATCTTCGGCTGA
Nod2(F): CAGGTCTCCGAGAGGGTACTG
Nod2(R): GCTACGGATGAGCCAAATGAAG
Sectm1a (F): TCAGTGCCTGCTATCCCTACC
Sectm1a (R): GGGGCTTTTTATCGAAGATGGT
Sectm1b (F): AGCCTCCCTGAATGCCTATAA
Sectm1b (R): ACGTCTCTGAGATTGTTGGAGAT
Icosl (F): TAAAGTGTCCCTGTTTTGTGTCC
Icosl (R): ATTGCACCGACTTCAGTCTCT
Ifngr1 (F): CTGGCAGGATGATTCTGCTGG

Ifngr1 (R): GCATACGACAGGGTTCAAGTTAT
Ifngr2 (F): TCCTCGCCAGACTCGTTTTC
Ifngr2 (R): GTCTTGGGTCATTGCTGGAAG
Hmgcs2 (F): ATACCACCAACGCCTGTTATGG
Hmgcs2 (R): CAATGTCACCACAGACCACCAG
H2-Ab1 (F): AGCCCCATCACTGTGGAGT
H2-Ab1 (R): GATGCCGCTCAACATCTTGC
H2-Aa (F): TCAGTCGCAGACGGTGTTTAT
H2-Aa (R): GGGGGCTGGAATCTCAGGT
Jag1 (F): CCTCGGGTCAGTTTGAGCTG
Jag1 (R): CCTTGAGGCACACTTTGAAGTA
Lgr5 (F): CCTACTCGAAGACTTACCCAGT
Lgr5 (R): GCATTGGGGTGAATGATAGCA